Application of satellite radar interferometry in study of the relation between surface deformation and seismic event of the 15th September 2018 in the Rudna copper mine, Poland

Karolina Owczarz, Jan Blachowski

Wrocław University of Science and Technology, Faculty of Geoengineering, Mining and Geology, Wrocław, Poland

ABSTRACT:

The phenomenon of induced seismicity is caused by anthropogenic activity such as: underground and opencast mining, extraction of conventional and unconventional hydrocarbons, construction of water reservoirs and production of geothermal energy. In recent years, interest in induced seismicity increased due to the fact that it causes increasingly stronger earthquakes, even above 4 on the Richter scale. Thus, it poses a threat to people, technical and urban infrastructure. This study analyzed the seismic event of M = 4.6, which occurred on the 15 September 2018 in the Rudna copper mine area in SW Poland. For this purpose, Sentinel 1 satellite data and DInSAR processing method were used to determine the ground movement values in the satellite line of sight. Based on the results for four image pairs, the area disturbed by the seismic event was determined. The maximum values of subsidence ranged from -65 mm to -75 mm depending on the analysed dataset and the area of deformation was determined at approx. 4 km sq. The results indicate the usefulness of the adopted method to determine ground deformation caused by induced seismicity in an underground mining area.

1 Introduction

Induced seismicity is an anthropogenic phenomenon, which manifests itself as shaking of earth of various magnitudes arising from the action of man on the surface or in the rock mass. Most seismic events are associated with underground and surface mining, as the technological processes used to extract raw material disturb the natural state of balance in the rock mass (Wilson et al., 2017; Foulger et al., 2018). In addition to mining, induced seismicity occurs, among other things, during hydraulic fracturing, construction of water reservoirs, underground storage of substances or production of geothermal energy. Depending on the technological process and the geological structure, at least four types of induced seismicity can be determined, such as: graviquakes, reinjection quakes, hydrofracturing quakes and load quakes (Doglioni, 2018). In all of these cases, the following factors play an important role: hydrostatic and lithostatic pressures, stresses and the occurrence of tectonic faults in places of anthropogenic activities. Each environment is characterized by special features, so knowledge of the mechanisms taking place is important to take appropriate precautions in industrial processes. The phenomenon of induced seismicity is not only a problem of the mining industry, but also a human safety and economic problem, because strong seismic shocks often damage technical and urban infrastructure on the surface, and in the consequence may lead to the death of people (Li et al., 2007; Avouac, 2012; Keranen et al., 2013; Rudziński et al., 2016; Gibbens, 2017).

Due to the strong influence of induced seismicity on various aspects of life, this phenomenon is a frequent subject of scientific research in order to determine the causes, course and effects. This article will focus on analysis of surface movements associated with seismic activity triggered by underground mining using satellite radar interferometry. The application of SAR technique in the studies of induced seismicity is a fairly recent topic, which still requires further research. In recent years there have been publications on this subject. Noteworthy studies include: Barba et al., 2016; Loesch and Sagan, 2017; Zhang et al., 2017; Krawczyk and Grzybek, 2018. The first team studied four regions in the USA: Greely, CO, Platteville, CO, Edmond, OK and Jones, OK, where induced seismicity is associated with fluid injection. The earthquakes triggered in these areas were of magnitude $M \geq 3$. The authors developed interferograms, based on satellite imagery with Radarsat-1/2, ERS-1/2, Envisat, ALOS and Sentinel-1 using the MSBAS algorithm. The aimed at identifying past and recent deformations to implement measures to mitigate induced seismicity. Similar research was carried out by a team in Oklahoma, where injection mining to extract oil is used and causes increased seismicity. The researchers used PALSAR satellite data and SBAS processing method to determine the spatial correlation between locations of deformation of wells. Zhang et al. investigated land subsidence in a potassium salt mine in Texas. For this purpose, they processed the ALOS PALSAR and Sentinel-1 data using the InSAR method. They observed a strong correlation between mining activities and settlement locations. Krawczyk and Grzybek focused on the area of the Upper Silesian Coal Basin, one of the areas of mining induced seismicity in Poland. The authors focused on determining the correlation between the range of surface deformations and the location of the epicenter of induced shocks. They used Sentinel-1 radar images and the InSAR method.

The content of this article contains the results of research on the application of satellite radar interferometry and data from Sentinel-1 mission to determine the surface deformations caused by the seismic event that occurred on the 15th of September 2018 in the vicinity of the underground copper ore mine Rudna in SW Poland. The shock that was triggered had magnitude of M=4.6. The paper is composed of the following sections: description of the area of the event, description of methodolo-

gy SAR data processing with DInSAR algorithm (Differential Synthetic Aperture Radar Interferometry), analysis and discussion of the results and conclusions.

2 Study area

The study focuses on one of the mining ground in the area of underground mining of copper ore in the Lower Silesia region (SW Poland) close to the border with Germany (Saxony). The deposits are associated with the Zechstein copper-bearing formation, consisting of white sandstones, limestone, and copper-bearing shale (Polish Geological Institute, 2019). The mines, including the analysed Rudna mine area, are the largest copper operations in Europe and one of the largest underground operations of this kind in the World. The deposit layers extend in the NW-SE direction following the course of the Fore-sudetic monocline boundary with the Fore-sudetic Block and dip towards the NE at an angle of 1 to 6 degrees. The Rudna copper deposit is characterized by a thickness of up to several meters, with an average thickness of just over 4 m (Oszczepalski et al., 2016).

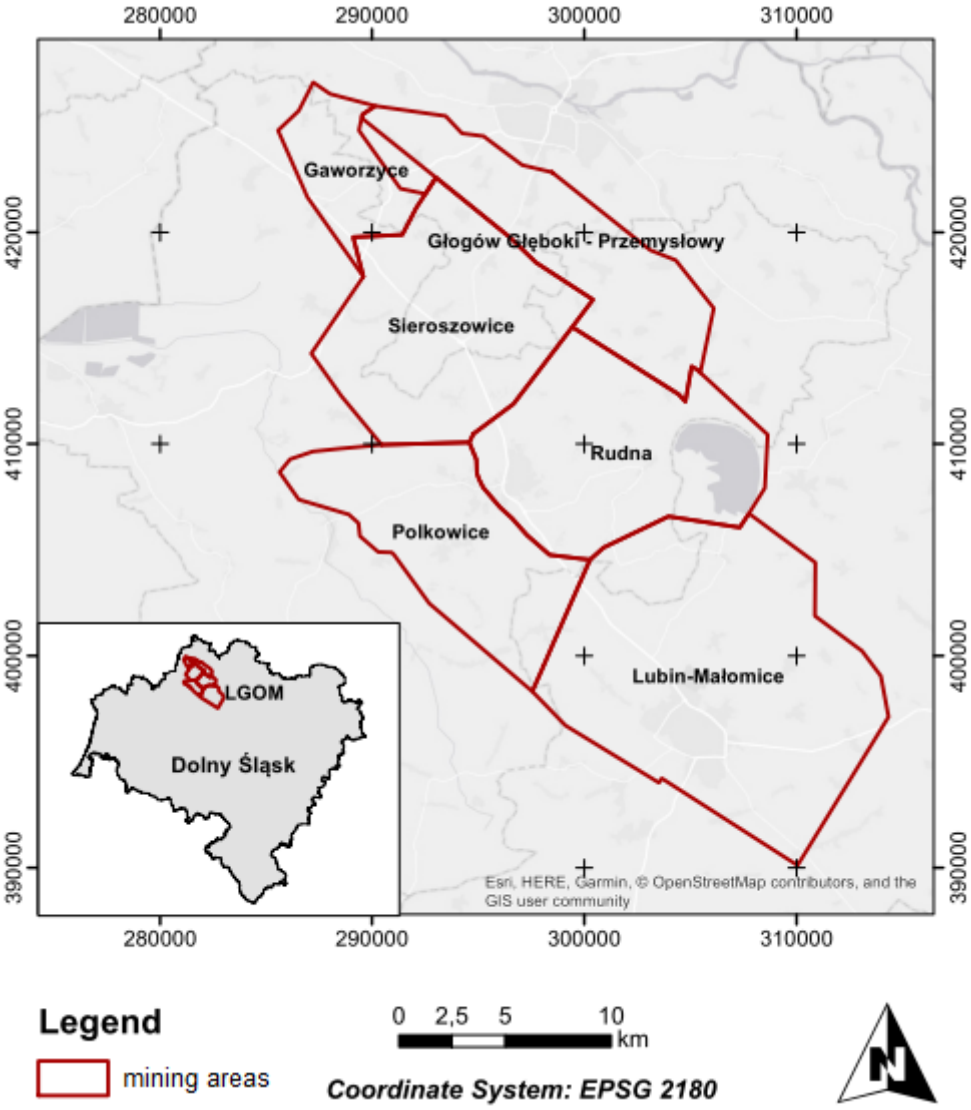

Fig. 1: Area of interest – Rudna copper mine

In the Rudna deposit, The depth of the of copper-bearing formations ranges from 844 to 1250 m below the terrain surface. There are numerous fault zones of various sizes and amplitudes in the area. These faults extend generally in the NW-SE direction. The deposit is mined with the room-and-pillar mining systems with the use of blasting (Konopacka and Zagożdżon, 2014). In this mining system the body of the deposit is cut by the rooms and strips with separated technological pillars. Continuous mining operation affects the natural state of the surrounding rock mass and frequently is responsible for seismic activity of various magnitude (above 4). The depth of Rudna deposit means that the threat of seismic shocks there is the highest among all the copper mines in the area. In 2018 alone there were 6 seismic shocks with magnitude of $M \geq 4$ associated with copper mining.

3 Data

Information on the date, location and magnitude of shocks was obtained from the European Mediterranean Seismological Center (EMSC), which collects parametric data in real time provided by 70 seismological networks from the Mediterranean region. There is local seismic network in the Rudna mine with more precise parametric data, but access to the data is restricted, which is why generally available data were used. Table 1 contains information about the analysed seismic event.

Tab. 1: Basic information about the analysed shock (EMSC, 2018)

Date and time UTC	Latitude [degrees]	Longitude [degrees]	Depth [km]	Magnitude
2018-09-15 16:35:15.3	51.57 N	16.14 E	2	4.6

In order to calculate the surface displacements caused by the analysed event, satellite images from Sentinel-1A and 1B missions were used. These are twin satellites, and their repeat time over the same location on earth is 6 days. The relatively short time for obtaining radar images and frequency of acquisitions makes it a good data source for studies of natural and human induced deformations of the Earth's surface. The satellites are equipped with synthetic aperture radar (SAR) sensors in the C band, which allow measurements in all weather conditions and at any time of the day. Four measuring modes (Stripmap - SM, Wave Mode - WV, Interferometric Wide swath - IW and Extra Wide swath - EW) provide several products (Raw Data, Ground Range Detected - GRD, Single Look Complex - SLC, Ocean - OCN) on three levels (Level-0, Level-1 SLC, Level-1 GRD, and Level-2 OCN). Access to all Sentinel-1 products is open. To determine surface displacements, the SLC product, which contains information on the phase and amplitude of the electromagnetic wave, is used. For the purpose of this research, several SLC satellite data pairs were acquired to perform calculations based on various time combinations. Figure 2 shows the analysed time combinations of satellite imagery in the DInSAR method, which will not cause a significant decrease in the coherence value between the two images.

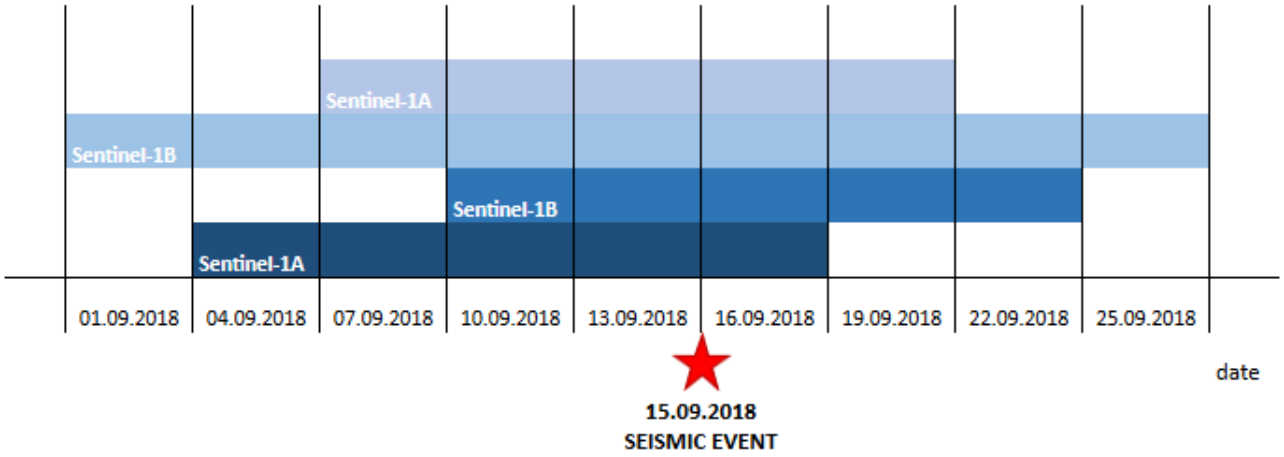

Fig. 2: Time combinations of satellite imagery in the DInSAR method used in the study

Satellite imagery was downloaded from the website www.scihub.copernicus.eu, which offers all products of the Sentinel mission. The images closest to the time of seismic event were used, prior and after the shock to construct possible data pairs. Pairs of satellite imagery selected for the study are presented in the table 2.

Tab. 2: Satellite imagery processed using the DInSAR method

Date of the event	Date of satellite imagery pairs		Sentinel-1	Type of orbit	Track
15.09.2018	1	2018-09-04 and 2018-09-16	A	descending	22
	2	2018-09-10 and 2018-09-22	B	descending	22
	3	2018-09-01 and 2018-09-25	B	ascending	73
	4	2018-09-07 and 2018-09-19	A	ascending	73

4 Methodology

In the research, the Differential Satellite Interferometry (DInSAR) method was used to determine the ground surface movement before and after the seismic event. The method is said to provide accuracy better than a centimeter (Burgmann et al., 2000; Wojciechowski and Perski, 2008; De et al., 2016). DInSAR is one of the methods of processing satellite imagery used to determine displacements caused, among other things by: earthquakes, mining exploitation, volcanic eruptions, tectonic movements, landslides (Karimzadeh et al., 2011; Saranya and Vani, 2017; Ishwar and Kumar, 2017; Huang et al., 2017; Syahreza et al., 2018). This method is based on acquiring the phase of the signal returning during the first and second satellite flight over the same place on earth. With such data available, it is possible to determine the phase difference, the value of which indicates the occurrence of movement of the terrain shown in the differential interferogram. The bands in the interferogram show the size of the displacement, where their full sequence indicates the movement of the area to or from the satellite (in the Line of Sight, LOS), which is equal to half the length of the electromagnetic wave (in Sentinel-1 λ = 5.6 cm). The DInSAR method is based on strictly defined processing steps, which are presented below.

Stage 1: Downloading a pair of satellite imagery that should meet the following conditions:

- both radar images made by the same satellite,
- perpendicular baseline below 300 m (the smaller the perpendicular baseline, the smaller the influence of the topography on the value of the phase difference),
- both radar images acquired for ascending or descending orbit.

DInSAR processing requires also digital elevation model SRTM and information about satellite orbits.

Stage 2: Coregistration of satellite imagery - involves matching the geometry of two SAR images to accurately determine the phase difference and reduce noise. This stage includes:

- coarse coregistration - searching for slave image shifts, matching two photos with an accuracy of one or two pixels,
- fine coregistration - search for link points with sub-pixel accuracy and resampling of the slave image.

Stage 3: Creating a synthesized interferogram, which involves generating an interferogram based on the digital elevation model and orbital information in order to remove the component responsible for the topography from the phase.

Stage 4: Creating the differential interferogram, which is the difference between the interferogram created from two SAR images and the synthesized interferogram. This procedure eliminates the component responsible for the topography from the phase to highlight the deformation component. The interferogram consists of interference fringes, which determine the terrain deformation equal to half the length of the electromagnetic wave.

Stage 5: Creating the coherence map to determine the consistency of the phase of signals between two SAR images. Coherence contains values ranging from 0 (lack of coherence) to 1 (full coherence). On the basis of the coherence map it is possible to interpret the interferogram as it indicates the places where the calculated deformations are reliable.

Stage 6: Interferogram filtering, which is the process of reducing noise in the intereferometric phase, which arises due to atmospheric factors, satellite image acquisition errors, temporal and spatial decorrelation and radar signal errors. Filtering affects the quality of phase unwrapping.

Stage 7: Phase unwrapping, this is an important process during the processing of satellite imagery, because it generates the absolute value of the phase that is used to determine the value of the deformation. A multiple of 2π is added to each original phase cycle value to reconstruct the original phase values of the signal.

Step 8: Creating a Line of Sight (LOS) displacement map - this is the last stage, in which the phase expansion values in radians are converted into relative values of displacements in millimeters towards the satellite Line of Sight (LOS).

The procedure of the DInSAR method described was used to calculate the deformation of the area in the neighborhood of the seismic event, which took place on the 15th of September 2018 at the Rudna mine. The results and their analysis are presented in the next section.

5 Analysis of the seismic event of 15th September 2018

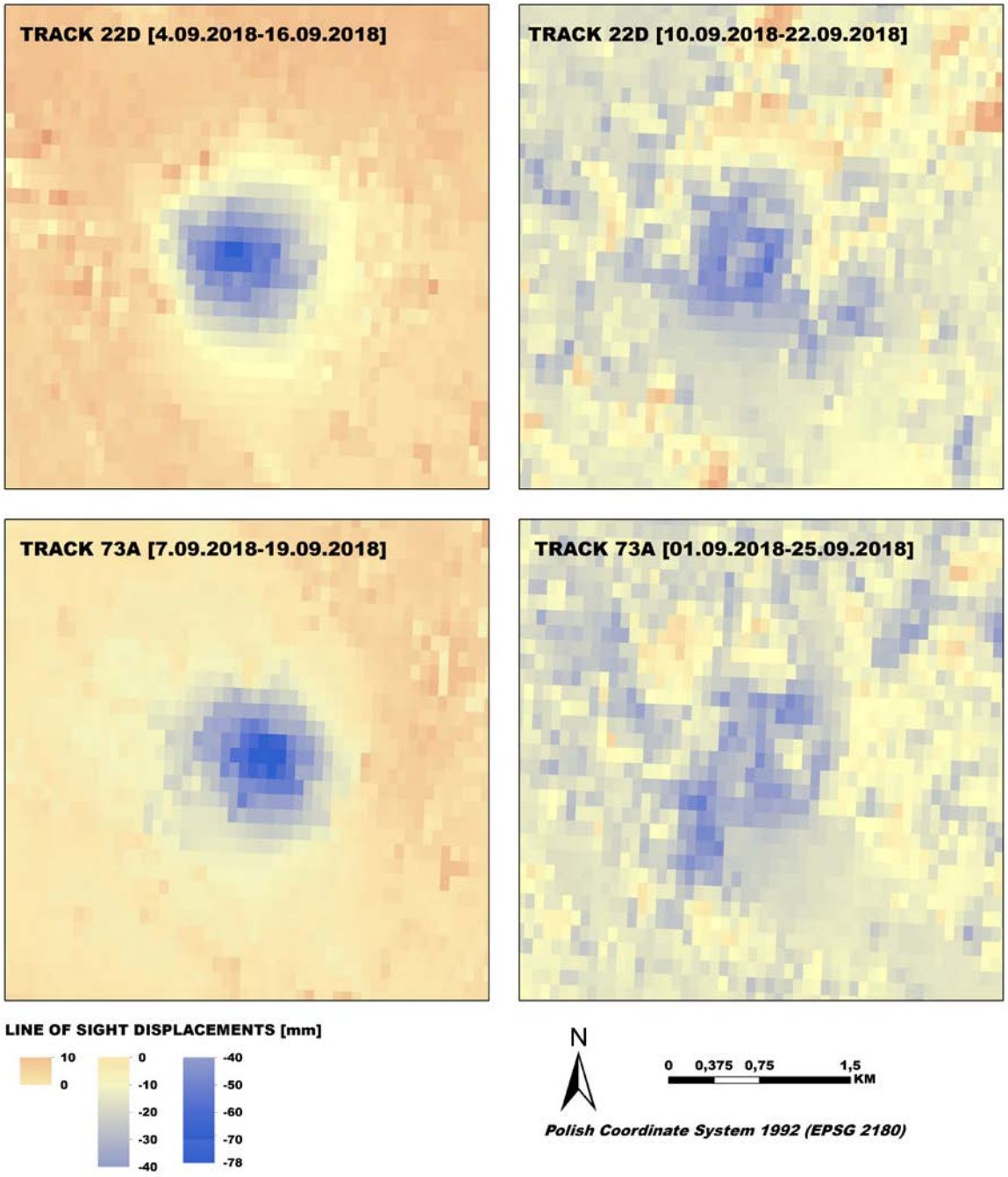

Fig. 3: Line of sight displacement maps for the analysed SAR data pair. Event of 15th September 2018

For this event four SAR radarogram pairs were processed and the resulting coherence and line of sight displacements analysed. The available radarogram pairs were: 1) 4-16.09.2018, and 2) 10-22.09.2018 for satellite track 22 (descending orbits) and 7-19.09.2018, and 9-23.09.2018 for satellite track 73 (ascending orbits).

The mean coherence value for the analysed area was relatively low, i.e. 0,29 with the maximum value of 0,98. Two of the data pairs. i.e. 10-22.09.2018 (track 22 descending orbit) and9-23.09.2018 (track 73 ascending orbit) were rejected because of these unsatisfactory coherence values. The other

two pairs, i.e. 4-16.09.2018 (track 22 descending orbit) and 7-19.09.2018 (track 73 ascending orbit) produced clear and corresponding results in terms of both the displacement values and displacement shape and horizontal extent. Line of sight displacement maps for all the data pair are shown in Fig 3. The maximum displacement for track 22D was approx. -65 mm and for track 73A approx. -75 mm. Thus, taking into consideration the expected accuracy of DInSAR technique (Burgmann et al., 2000; Wojciechowski and Perski, 2008; De et al., 2016) the 4.6 magnitude seismic event is responsible for approx. -70 mm of subsidence.

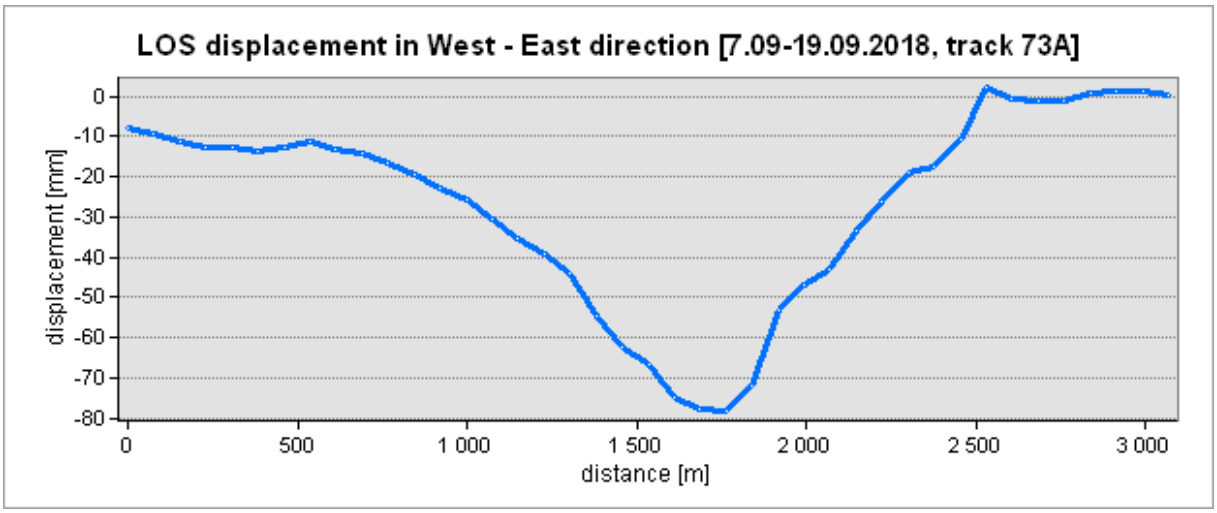

Fig. 4: W-E cross-section through the analysed area for the 7.09-19.09.2018 and track 73A data pair

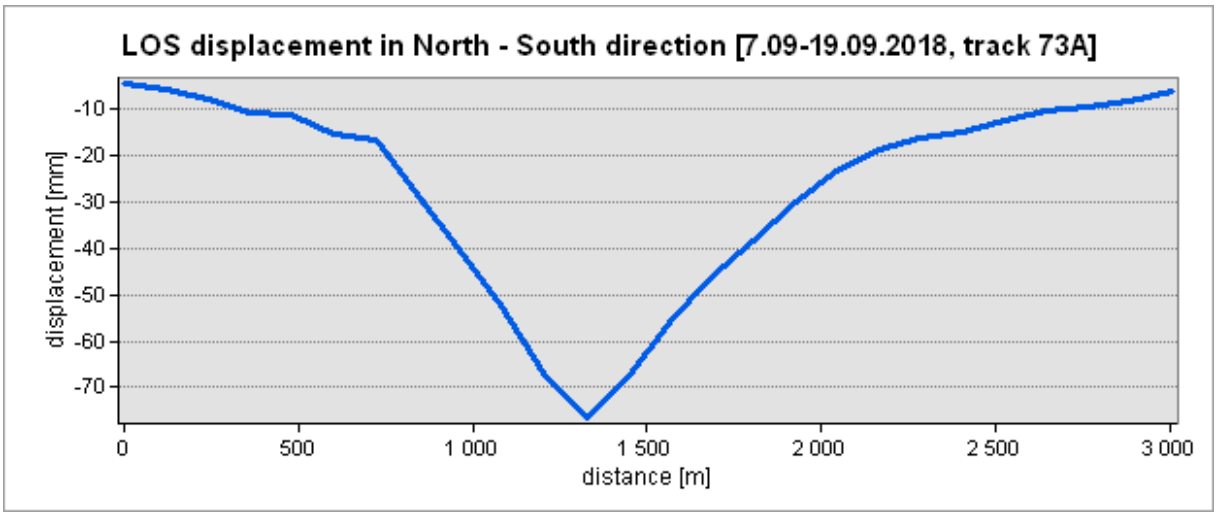

Fig. 5: N-S cross-section through the analysed area for the 7.09-19.09.2018 and track 73A data pair

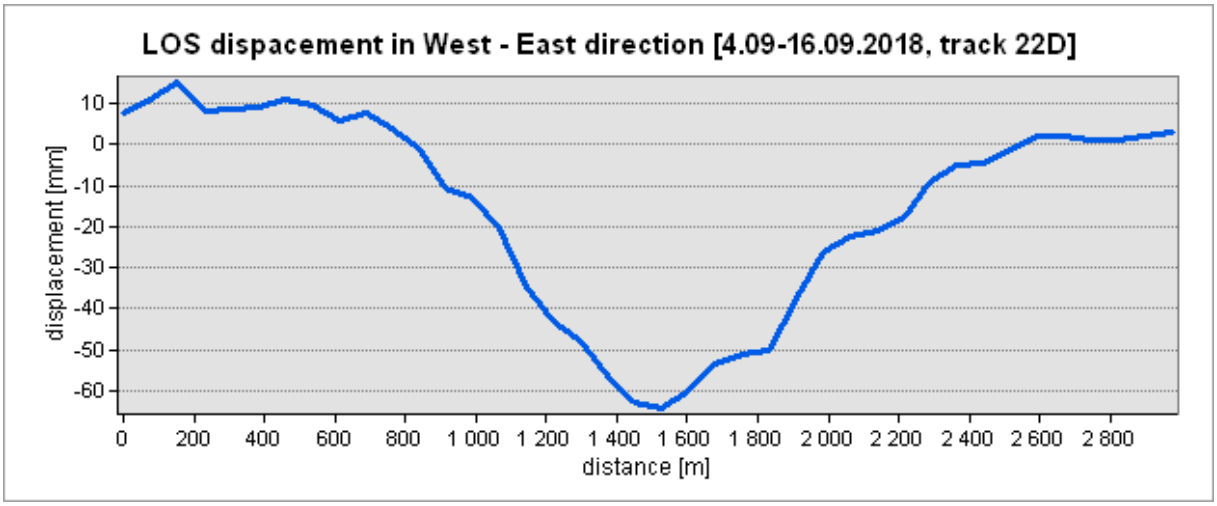

Fig. 6: W-E cross-section through the analysed area for the 4.09-16.09.2018 and track 22D data pair

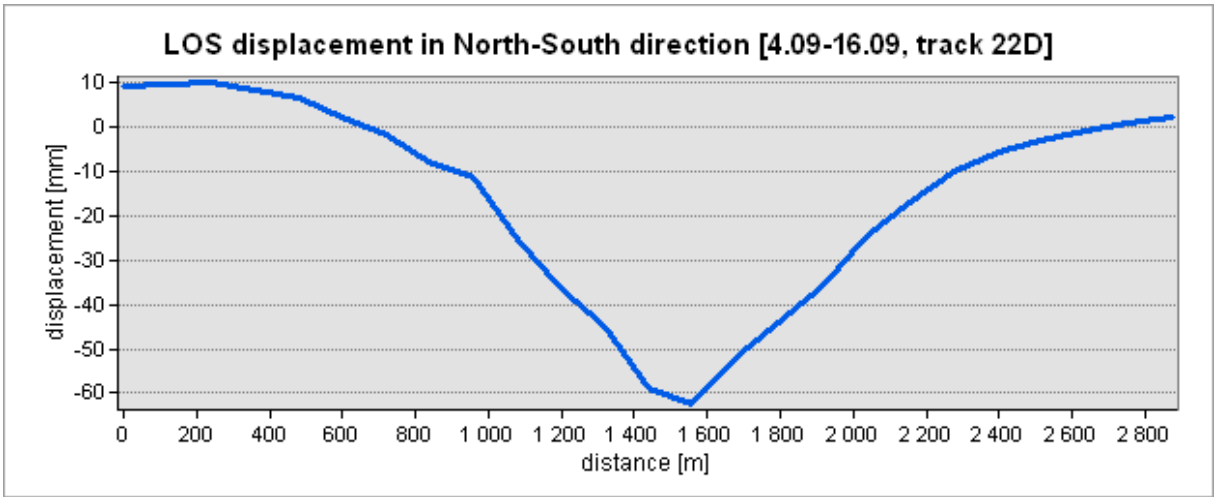

Fig. 7: N-S cross-section through the analysed area for the 4.09-16.09.2018 and track 22D data pair

The frequency of Sentinel 1A/B radarogram acquisitions (12 days for a satellite and 6 days when two satellites are used) allows for multiple data pairs for the date of the seismic event. Multiple and separate interferograms and Line of sight displacement maps that can be obtained thorough processing of these data pairs allow for verification of displacement calculations (separate for each data pair) to accommodate for the geodetic measurements that because of the sudden and unexpected character of the induced seismicity process are not present. In the discussed case at least four different datasets from two different satellite tracks were available for DinSAR processing. This allows also to accommodate for possible low coherence of some data pairs (longer temporal base, possible effect of atmospheric errors, etc.).

Generalised shape of the subsidence area modelled with IDW interpolation method based on input discrete points from centroid of the LOS displacement raster is shown in Fig. 8.

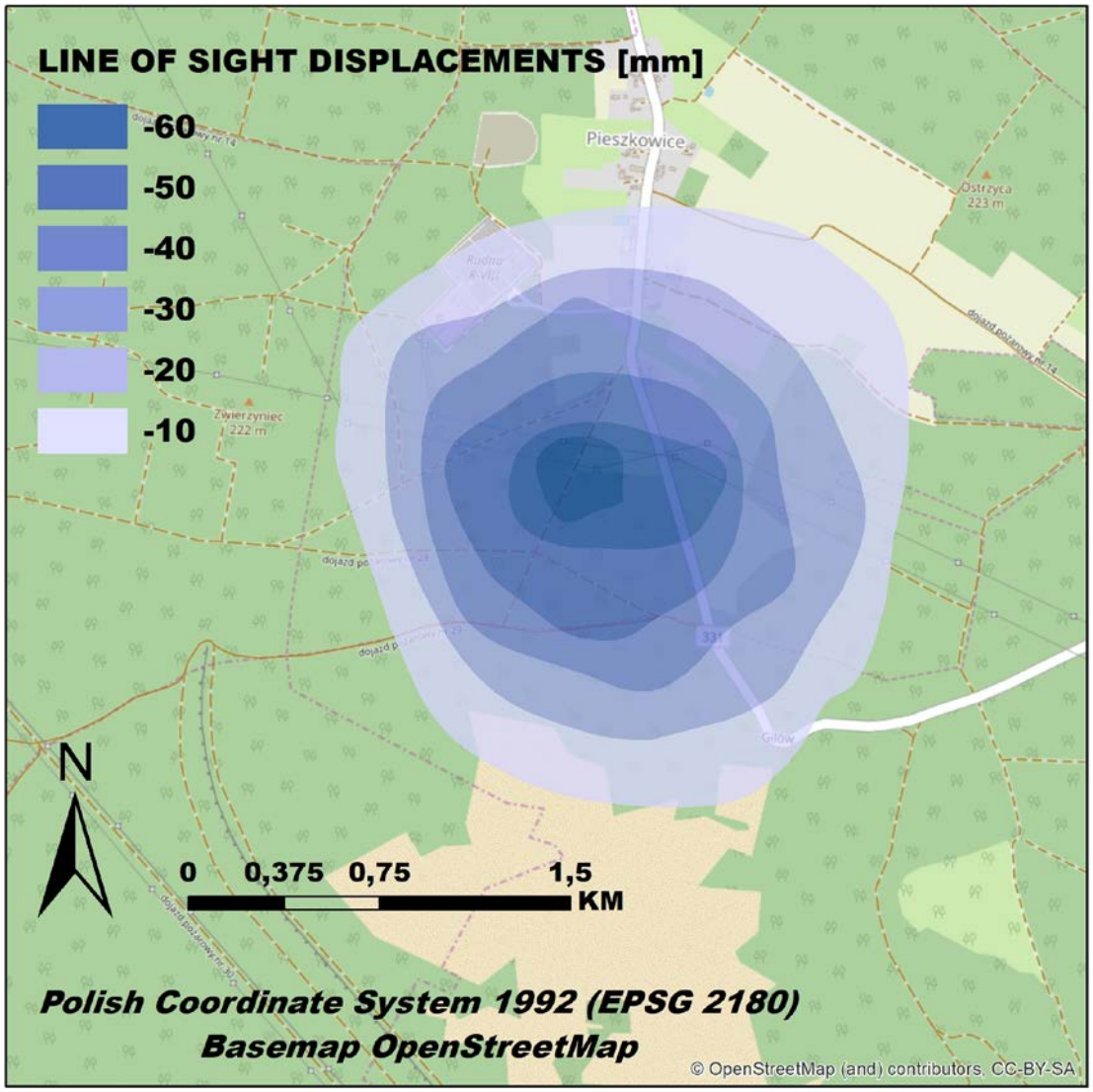

Fig. 8: Extent of the subsidence area caused by seismic event of the 15th September 2018

6 Conclusions

In the research, the ground movement caused by the seismic event of 15 September 2018 with magnitude M = 4.6, which occurred in the Rudna underground copper mine area, were determined and located on the surface. For this purpose, the method of differential satellite interferometry (DInSAR) was used, which is appropriate for determining land movement between two subsequent satellite data acquisition. The results indicate land subsidence caused by the seisimic event, with maximum values at the centre of the subsidence bowl from -65 mm to -75 mm depending on the analysed pair of images. The extent of the identified deformation area is approx. 2 km x 2 km. Out of the four image pairs analysed two produced accurate results, whereas the other two the other two pairs, due to the large time interval and lack of coherence, did not generate the expected results. In addition to the factors mentioned above, atmospheric factors, which are hard to eliminate from the phase components, could have influenced these results. Similar LOS displacement results for two image pairs validate the extent of surface deformations.

The use of the DInSAR method and the Sentinel-1 satellite imagery provides the opportunity to obtain information on the effects of induced seismicity on the surface in a relatively short time, for large areas and for events that took place in the past. The frequency of Sentinel SAR data acquisi-

tions makes it possible to investigate the phenomenon of mine induced seismicity that previously was very difficult due to the lack of measurement data collected prior to a seismic event.
Monitoring of the effects of induced seismicity on the surface provides information that leads to extending the knowledge about these events and their influence on the state of the ground. Performing geodetic and satellite measurements, as well as analyzing their results in relation to geological structure and mining plans can be a major contribution to the development of preventive measures mitigating negative consequences of induced seismicity.

REFERENCES

Avouac, J.P: Human-induced shaking. NATURE GEOSCIENCE ADVANCE ONLINE PUBLICATION, 2012

Barba, M.; Tiampo, K. F.; Samsonov, S. V., InSAR MSBAS Time-Series Analysis of Induced Seismicity in Colorado and Oklahoma. Americam Geophysical Union, Fall Meeting, 2016.

Burgmann, R.; Rosen, P.A.; Fielding, E.J.: SYNTHETIC APERTURE RADAR INTERFEROMETRY TO MEASURE EARTH'S SURFACE TOPOGRAPHY AND ITS DEFORMATION, Annu. Rev. Earth Planet. Sci., Vol. 28, pp. 169–209, 2000.

Doglioni, C.: A classification of induced seismicity. Geoscience Frontiers, Vol. 9, pp.1903-1909, 2018.

Foulger, G.R.; Wilson, M.P.; Gluyas J.G; Julian B.R.; Davies R.J: Global review of human-induced earthquakes, Earth-Science Reviews, Vol. 178, pp. 438-514, 2018.

Gibbens, Sarah: How Humans Are Causing Deadly Earthquakes, National Geographic, 2017.

Huang, J.; Xie, M.; Farooq, A.; Williams, E.J.: DInSAR technique for slow-moving landslide monitoring based on slope units. Survey Review, 2017.

Ishwar, S.G.; Kumar, D.: Application of DInSAR in Mine Surface Subsidence Monitoring and Prediction. Current Science, vol. 112, pp. 46-51, 2017.

Karimzadeh, S.; Osmanoglu, B.; Mansouri, B.; Djamour, Y.: Application of Differential SAR Interferometry (DInSAR) for Interseismic Assessment of North Tabriz Fault, Iran. 1st International Conference on Urban Construction in the Vicinity of Active Faults, 2011.

Keranen,K.M.; Savage,H.M.; Abers, G.A.; Cochran,S.E.: Potentially induced earthquakes in Oklahoma, USA: Links between wastewater injection and the 2011 Mw 5.7 earthquake sequence, Geology, Vol. 41, pp. 699-702, 2013.

Konopacka, Ż.; Zagożdżon, K.D.:Łupek miedzionośny Legnicko-Głogowskiego Okręgu Miedziowego. Monografia Politechniki Wrocławskiej, Wydział Geoinżynierii, Górnictwa i Geologii, 2014 (in Polish)

Krawczyk, A.; Grzybek, R.: An evaluation of processing InSAR Sentinel-1A/B data for correlation of mining subsidence with mining induced tremors in the Upper Silesian Coal Basin (Poland), E3S Web Conf., Vol. 26, 2018.

Li, T.; Cai, M.F.; Cai, M.: A review of mining-induced seismicity in China, International Journal of Rock Mechanics and Mining Sciences, Vol. 44, pp. 1149-1171, 2007.

Loesch, E.; Sagan, V.: SBAS Analysis of Induced Ground Surface Deformation from Wastewater Injection in East Central Oklahoma, USA. Remote Sens., Vol. 10, 2018.

Luca, C.D.; Bonano, M.: Casu, F.; Fusco, A.; Lanari, R.; Manunta, M.; Manzo, M.; Pepe, A.; Zinno, I.: Automatic and Systematic Sentinel-1 SBAS-DInSAR Processing Chain for Deformation Time-series Generation. Procedia Computer Science, Vol. 100, pp. 1176-1180, 2016.

Oszczepalski, S.; Speczik, S.; Małecka, K.; Chmielewski, A.: Prospective copper resources in Poland. Gogospodarka surowcami mineralnymi – mineral resources management, Vol. 32, pp. 5-30, 2016.

Rudziński, Ł.; Cesca, S.; Lizurek, G.: Complex Rupture Process of the 19 March 2013, Rudna Mine (Poland) Induced Seismic Event and Collapse in the Light of Local and Regional Moment Tensor Inversion. Seismological Research Letters, Vol. 87, pp. 274-284, 2016.

Saranya, P.; Vani, K.: Deformation Monitoring of Volcanic Eruption Using DInSAR Method.

Computational Intelligence in Data Mining pp. 715-727, 2017.

Syahreza, S.; Fadhli; Saepuloh, A.; Lateh, J. and H.: Combining the Sentinel-1A/B DinSAR Interferometry to Detect Deformation Associated with Pidie Jaya Earthquake. The 8th International Conference on Theoretical and Applied Physics, 2018.

Wilson,M.P.; Foulger,G.R.; Gluyas,J.G.; Davies,R.J; Julian,B.R.: HiQuake:The Human – Induced Earthquake Database. Seismological research letters, Vol. 88, pp.1560-1565, 2017.

Wojciechowski, T.; Perski, Z.: ZASTOSOWANIE SATELITARNEJ INTERFEROMETRII RADAROWEJ DO OKREŚLENIA AKTYWNOŚCI OSUWISK OBRZEŻENIA KOTLINY SĄDECKIEJ. Archiwum Fotogrametrii, Kartografii i Teledetekcji, Vol. 18, 2008 (in Polish with English summary)

Zhang, A.; Lua, J.; Kim, J.W.: Detecting mining-induced ground deformation and associated hazards using spaceborne InSAR techniques. Geomatics, Natural Hazards and Risk, Vol. 9, 2018.